Supporting Information: Band alignment and defects influence the electron-phonon heat transport mechanisms across metal interfaces

David H. Olson,[1] Maria G. Sales,[2] John A. Tomko,[2] Teng-Fei Lu,[3] Oleg V. Prezhdo,[4] Stephen J. McDonnell,[2] and Patrick E. Hopkins[1,2,5,a]

[1]*Department of Mechanical and Aerospace Engineering, University of Virginia, Charlottesville, VA 22904, USA*

[2]*Department of Materials Science and Engineering, University of Virginia, Charlottesville, VA 22904, USA*

[3]*School of Materials Science and Engineering, Dalian Jiaotong University, Dalian 116028, Liaoning Province, China*

[4]*Department of Chemistry, University of Southern California, Los Angeles, California 90089, USA*

[5]*Department of Physics, University of Virginia, Charlottesville, VA 22904, USA*

[a]phopkins@virginia.edu

S1. TIME-DOMAIN THERMOREFLECTANCE

In time-domain thermoreflectance (TDTR), 100 fs pulses emanate from an 80 MHz Ti:Sapphire oscillator, centered at 800 nm (1.55 eV) with a bandwidth of ~11.5 nm. In our implementation, we frequency-double the pump to 400 nm (3.1 eV) using a $BiBO_3$ crystal to increase absorption in Au. The probe is mechanically delayed in time to monitor the thermoreflectance at the sample surface. The $1/e^2$ pump and probe radii are 8.0 and 4.5 μm, respectively, with the incident pump fluence being 3.85 J m^{-2} for the Au/TiO$_x$ films and 2.42 J m^{-2} for the Au film. The cross-correlation of the pump and probe pulses at the sample surface is ~800 fs[1] due to the dispersion induced from various components in the TDTR optical path.

S2. VARYING AU THICKNESS IN AU/TIO$_x$ SYSTEMS

The in-phase reflectivity responses (V_{in}) of Au/TiO$_x$ systems with varying Au thicknesses are presented in Fig. S1. In these specimens, a 5 nm TiO$_x$ layer was deposited in a moderately high vacuum ($< 1 \times 10^{-6}$) Torr at 1.0 Å/s, which ensured at least some fraction of the layer contained Ti^0 according to the main manuscript and our previous study.[2] The thickness of the Au layer was confirmed via X-ray reflectivity. Specimens with an Au capping layer of < 102 nm reveal a significant rerise in the acquired magnitude following initial peak indicative of the electron temperature. Those with very thin Au capping layers, 14 and 24 nm, reveal a sign change at ~2 ps where the signal goes negative before rerising again. We are unsure for the exact reasons for this, but hypothesize that it is related to the convolution of the Au and Ti thermoreflectance values at the probing wavelength. At the pump wavelength, a significant portion of optical energy is directly coupled to electrons in the Ti based on the optical skin depth of Au, ~16 nm.[3] As the electron and lattice contribution to thermoreflectance of TiO$_x$ is relatively unexplored, as well as its temperature dependent indices of refraction, we expect the signal acquired by the probe to be influenced by the Ti layer in some capacity. Nonetheless, we do not observe a sign change at thicknesses ≥ 49 nm, suggesting that this thickness may be optimal for interpreting the data via the TTM. For this reason, all specimens in the manuscript were coated with an Au layer of ~50 nm.

The characteristic electron-phonon interaction length is mathematically defined as $\lambda_{ep} = \sqrt{\kappa_e/g}$, where κ_e and g are the electronic thermal conductivity and electron-phonon coupling
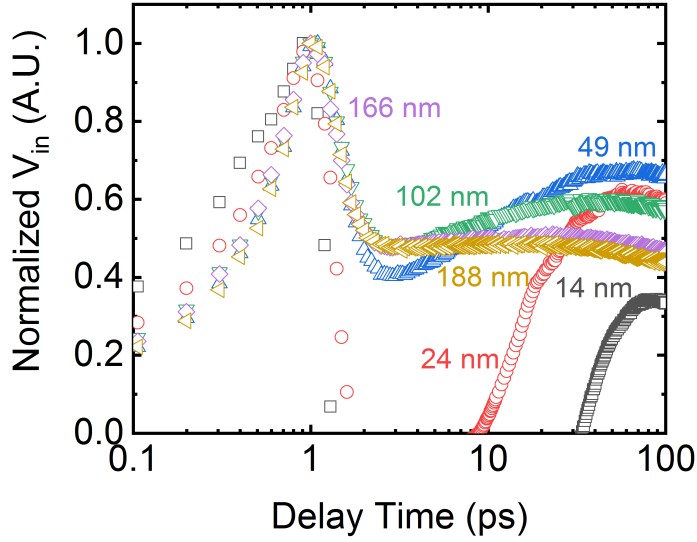
FIG. S1. Ultrafast response in Au/TiO$_x$ systems with varying Au thicknesses, labeled.

factor, respectively. In bulk Au, $\lambda_{ep} \approx 110$ nm.[4] Thus, performing these measurements with varying Au thickness yields critical insight into the interaction length between these two carriers. At an Au layer thickness of 166 nm, we observe a slight rerise in the signal, which is entirely diminished at 188 nm. At an Au thickness of 102 nm, the magnitude of this rerise is larger than at 166 nm, and at 49 nm the rerise is larger yet. For this rerise to occur, optically excited electrons in the Au layer must propagate through the Au layer without coupling with the lattice so that they can ballistically traverse into the TiO$_x$ layer. Once there, energy is transmitted to the lattice due to the ultrahigh g of the wetting layer, and the lattice temperature differential between the wetting and Au layers results in diffusion of heat via the lattice to the Au film, causing an increase in our acquired signal. If electrons are not able to reach the TiO$_x$ layer, then we would not expect a rerise in the signal. If we account for both the 1/e absorption depth at the pump wavelength, $\delta \approx 16$ nm,[3] as well as the characteristic electron-phonon interaction length, the length over which energy is deposited into the Au layer will be $\delta + \lambda_e \approx 126$ nm.[5] We find this value to be consistent with our experimental data, as it is less than the Au thickness at which we observe a diminished rerise in the signal, 166 nm, but larger than at 102 nm where the rerise is still present. Further experiments with finer increments in Au thickness would help to identify λ_e definitively.

S3. TWO-TEMPERATURE MODELING

To model the data acquired via TDTR, we first adjust the zero delay time of our TDTR data to be at approximately halfway of the initial peak to account for the delayed onset of electron thermalization. Spatial and temporal discretizations of 0.5 nm and 50 fs, respectively, are used in simulating the energy deposition. The substrate is modeled to be 100 nm, with a 0.5 nm discretization. The final discretized layer of the substrate is fixed to have an infinite heat capacity to emulate a semi-infinite substrate. The electronic heat capacity of each layer is chosen to be proportional to temperature via the electronic heat capacity coefficient γ, $C_e = \gamma T_e$, which is valid for the range of electronic temperatures in this study. The electron-phonon coupling factor g is approximately independent of lattice and electronic temperatures for low temperature perturbations,[4] and is thus chosen to be constant. Interfaces are modeled have thicknesses of 0.5 nm, where the phonon thermal conductance is given an equivalent thermal conductivity for the discretized thickness, and the electronic thermal conductance is the product of the average of the electronic temperatures on either side of the interface and Γ (i.e., $\Gamma T_{e,\text{ave}}$) to be in accordance with electron diffuse-mismatch model.[6] For systems with a wetting layer, we fix the Au/TiO$_x$ phonon conductance to 100 MW m^{-2} K^{-1}. Additionally, for 1 nm pure Ti, we use literature values[7] for the electron and phonon thermal conductivities, adjusted for size effects using kinetic theory. For 4 nm TiO$_x$ films, we assume 1 W m^{-1} K^{-1} for both the phonon thermal conductivity for amorphous TiO$_2$ films.[8] For the electron thermal conductivity in these films, 1 W m^{-1} K^{-1} is also assumed to account for any Ti^0 that may be present. See Table I of the manuscript for all inputs into the model.

In defining the electronic heat capacity, $C_e = \gamma T_e$, we choose to take γ for Ti from Lin et al.'s work[4] in describing those of our TiO$_x$ films. A more rigorous definition of γ, however, depends on the electron density of states at the Fermi level, $D(\epsilon_F)$, where ϵ_F is the Fermi energy. The electron heat capacity can be shown to be directly proportional to $D(\epsilon_F)$:[9]

$$C_e = \frac{\pi^2}{3} k_B^2 D(\epsilon_F) T_e = \gamma T_e. \tag{S1}$$

Examining the electron density of states for Ti$_x$O$_y$ from Fig. 4 of the main manuscript, there are several key features to note. At ϵ_F for Ti, a large electron density exists, which ultimately correlates to a large value of γ for Ti. In stoichiometric TiO$_2$, the electron density is nearly 0. However, in our TiO$_x$ systems in which $x \approx 2$, the presence of unreacted Ti^0, as confirmed via XPS and our two-temperature modeling, must provide additional states at and near ϵ_F, thereby

increasing γ. Thus, γ of pure Ti is chosen for TiO$_x$ films with $x \approx 2$. With regards to the TiO$_x$ layer with $x = 2.62$, we are unable to rigorously define γ due to the off-stoichiometry of the film. In examining the electron density of states for Ti$_3$O$_8$ in Fig. 4 of the manuscript, the number of states at ϵ_F is comparable to that of Au. This large number of states is the reason for the theoretically efficient electron energy transmission, as described by Γ, at Au/Ti$_3$O$_8$ interfaces shown in Fig. 3 of the manuscript. Further, $D(\epsilon_F)$ for Ti$_3$O$_8$, being comparable to that of Au, suggests that a value of γ similar to that of Au would best describe γ for Ti$_3$O$_8$. However, as the stoichiometry of TiO$_x$ for $x = 2.62$ is not exactly Ti$_3$O$_8$, we choose γ of pure Ti to describe our TiO$_{2.62}$ layer to allow for an intercomparison between all TiO$_x$ specimens.

Part of the analysis of the two-temperature model relies on the interpretation of the electronic and phononic temperatures described by the TTM. In general, the reflectivity is exhibits contributions from the electronic and lattice subsystems:[10]

$$\Delta R = a\Delta T_e + b\Delta T_l. \tag{S2}$$

In this equation, ΔR is the change in reflectivity resulting from perturbations in the electronic and lattice temperatures, ΔT_e and ΔT_l, respectively. The factors a and b are scaling constants that determine the contributions of each of these systems to ΔR. Because the signal acquired in TDTR encompasses contributions from both of these systems, and that the electronic contribution to thermoreflectivity becomes negligible $\sim$3 ps after excitation by the laser pulse near 800 nm for fluences used in this work,[11,12] we choose to interpret the lattice temperature acquired by the TTM and compare it to our measured data 3 ps after excitation. This interpretation accounts for the subsurface temperature profile and its influence on the thermoreflectivity,[13] where the temperature at each discrete point beneath the surface contributes to the reflectivity and approximately follows the optical attenuation depth. The weighting function, dR/dT, with which we use to interpret this subsurface temperature utilizes the index of refraction, n, of Au and its temperature dependence, dn/dT, at our probing wavelength, 800 nm, using previously reported data.[14] Because temperature dependent indices of refraction are not available for our TiO$_x$ films, nor would there be any reasonable way of determining them without compromising their current stoichiometry, we utilize those from Au in the determination of the weighting function in our analysis.

The dR/dT weighting function assuming the temperature dependent indices of refraction of Au for both the Au and TiO$_{1.90}$ layers is shown in Fig. S2(a) as the black solid line. The weighting function exemplifies the insensitivity of the contribution from the underlying TiO$_{1.90}$ layer, as

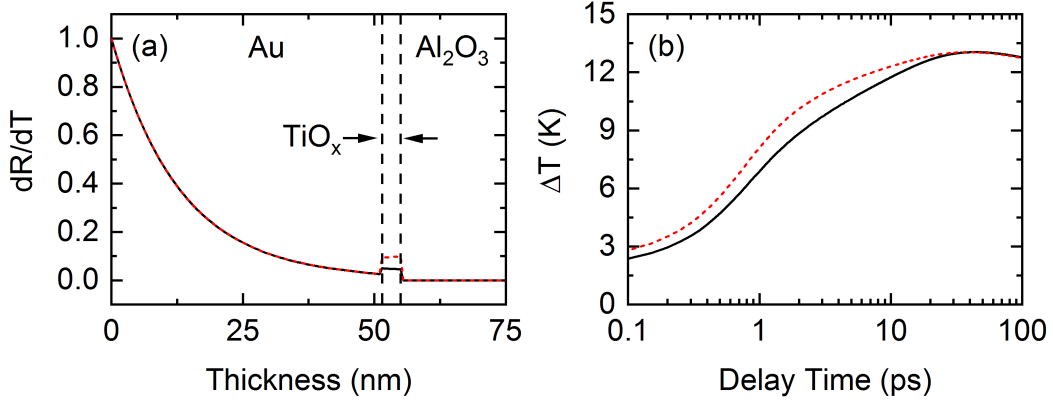FIG. S2. (a) dR/dT weighting function and (b) probe-averaged temperature response of the Au/4 nm TiO$_{1.90}$/Al$_2$O$_3$ system under the assumption that the temperature dependent indices of refraction of the TiO$_{1.90}$ layer are that of Au (black solid line) and Pt (dashed red line).

dR/dT is < 0.05 within this region. As an extreme example, we recalculate this weighting function under the assumption that the temperature dependent indices of refraction in the TiO$_x$ layer are that of Pt.[14] Shown as the dashed red line in Fig. S2(a), this results in a negligible change in the dR/dT weighting function–the majority of the contribution to the probe reflectivity is manifested in the Au capping layer. The probe-averaged temperature rise when utilizing both weighting functions is shown in Fig. S2(b). While a distinction can be made between these responses, we emphasize that we normalize and fit the model to our data beyond 3 ps, and that the rate at which the temperatures rise for each response are similar. Fitting our data under the assumption that the temperature coefficients of the TiO$_{1.90}$ layer are that of Pt provides similar lower bounds to g and Γ compared to when those of Au are used.

We note that for the time scales over which we determine the parameters of interest, we are not particularly sensitive to the Au/Al$_2$O$_3$ and TiO$_x$/Al$_2$O$_3$ phonon conductances in the Au/Al$_2$O$_3$ and Au/TiO$_x$/Al$_2$O$_3$ systems, respectively, due to the fact that thermal diffusion into the substrate typically occurs beyond $\sim$100 ps.[15] For the electron-phonon coupling factor of Au, uncertainty is determined by perturbing the pump and probe indices of refraction, the temperature dependent index of refraction of the probe, as well as the fluence by 10% and taking the difference between the newly acquired g and original g and calculating the quadrature. For g and Γ in systems with the TiO$_x$ adhesion layer, we determine the bounds to these values when the sum of the square of the difference between our data and the implemented TTM model (i.e., $\sum(T_d\text{-}T_m)^2$, where T_d is

the measured thermoreflectance data and T_m is the TTM model) is $< .02$ for the range over which the data are fitted.

S4.   THEORY AND SIMULATION DETAILS

A.   Time-Domain Density Functional Theory (TDDFT)

In real-time TDDFT, the electron density, $\rho(r,t)$, evolves in time and is obtained by summation over densities of the occupied time-dependent single-electron Kohn Sham (KS) orbitals, $\Psi_n(r,t)$:

$$\rho(r,t) = \sum_{n=1}^{N_e} |\Psi_n(r,t)|^2 \tag{S3}$$

where n = 1, 2, ..., N_e, and N_e is the total number of electrons. The equations of motions are obtained using the time-dependent variational principle applied to the total Kohn-Sham energy. Each evolving KS orbital satisfies the equation:

$$i\hbar \frac{\partial}{\partial t}\Psi_n(r,t) = H[\rho(r,t)]\Psi_n(r,t) \tag{S4}$$

where the Hamiltonian is a DFT functional that depends on the electron density, its gradient, etc. The equations are coupled, because $H[\rho(r,t)]$ depends on all KS orbitals. In order to solve the time-dependent KS (TDKS) equations, Eq. S4, we expand the time-dependent KS orbitals in the basis of adiabatic KS orbitals, $\Phi_k(r; \mathbf{R}(t))$, which are calculated by ground state DFT for the current nuclear coordinates $\mathbf{R}$,

$$\Psi_n(r,t) = \sum_k C_k^n(t)\Phi_k(r; \mathbf{R}(t)). \tag{S5}$$

Such expansion provides an efficient numerical way to solve the time-dependent KS equations, because adiabatic KS orbitals are available from many highly optimized DFT codes, and because the size of the expansion is small compared, for instance, to a grid representation in the position or momentum space. By insertion of Eq. S5 into Eq. S4, one converts the time-dependent KS equations into equations for the expansion coefficients:

$$i\hbar \frac{\partial}{\partial t}c_j^n(t) = \sum_k C_k^n(t)(\epsilon_k \delta_{jk} + d_{jk}) \tag{S6}$$

where ϵ_k is energy of the adiabatic KS orbital k, and d_{jk} is the nonadiabatic coupling (NAC) between adiabatic KS orbitals j and k. The NAC arises from atomic motions that change adiabatic

orbitals along a nuclear trajectory. We calculate the NAC numerically as the overlap between adiabatic orbitals j and k at sequential time steps:

$$d_{jk} = -i\hbar \frac{\langle \Phi_j | \nabla_R H | \Phi_k \rangle}{\epsilon_j - \epsilon_k} \cdot \frac{dR}{dt} = -i\hbar \langle \Phi_j | \nabla_R | \Phi_k \rangle \cdot \frac{dR}{dt} = -i\hbar \langle \Phi_j | \frac{\partial}{\partial t} | \Phi_k \rangle. \qquad \text{(S7)}$$

The current version of the above scheme is implemented[16,17] with the Quantum Espresso (QE) package.[18]

B.   Non-adiabatic Molecular Dynamics by Surface Hopping

Solution to the time-dependent Schrodinger equation, presently Eq. S4, provides input to surface hopping (SH). SH is needed in order to obtain branching and thermodynamic equilibrium, which are not trivial to achieve when the Schrodinger equation for electrons is coupled to a classical trajectory for atoms. In particular, a classical trajectory cannot branch, in contrast to quantum mechanical wave-packets, and the unitary evolution provided by the Schrodinger equation cannot reach thermodynamic equilibrium which requires coupling to a bath. Fewest switches SH (FSSH) developed by Tully[19] is a very popular and efficient SH strategy. The scheme minimizes the number of hops and defines the SH probability using population fluxes between quantum states. The time-dependent probability of a hop from state j to state k within the time interval dt is given in FSSH by:

$$dP_{jk} = \frac{-2Re(A_{jk}^* d_{jk}\dot{\mathbf{R}})}{A_{jj}} dt$$

$$A_{jk} = c_j c_k^*. \qquad \text{(S8)}$$

If the hopping probability dP_{jk} is negative, it is set to zero: a hop from state j to state k is allowed to take place only when the electronic occupation of state k increases and the occupation of state j decreases. A random number distributed uniformly between 0 and 1 is sampled and compared to the hopping probability in order to determine whether the system should remain in the current state or should hop to a new state. When an electronic transition occurs, the original FSSH technique rescales the nuclear velocities along the NAC direction to conserve the total electron-nuclear energy. If there is not enough nuclear kinetic associated with the NAC direction to account for the increase in the electronic energy, the hop is rejected. The velocity rescaling and hop rejection rules give detailed balance between transitions upward and downward in energy, mimicking Boltzmann
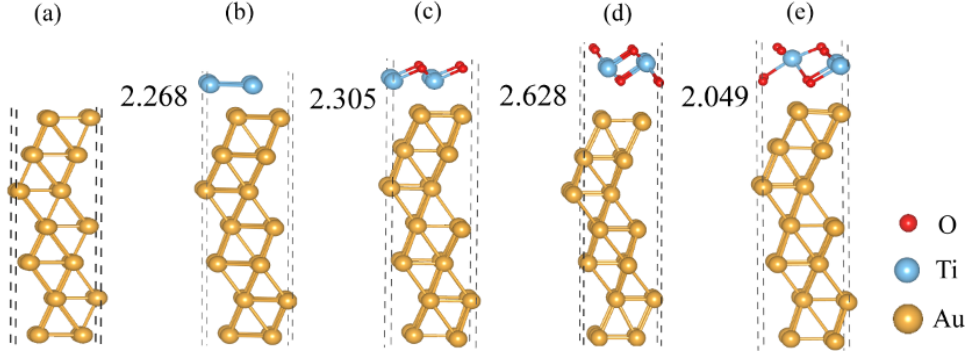
FIG. S3. Geometries of (a) pure Au(111) slab, and Au(111) slab with absorbed (b) Ti, (c) Ti_4O_4, (d) Ti_4O_8 and (e) Ti_3O_8 layers at 0 K. The numbers on the left side of the structures indicate the distances between the TiO_x layer and the nearest Au layer.

statistics and leading to quantum-classical thermodynamic equilibrium at long times. Under the classical path approximation, the velocity rescaling and hop rejection are replaced by multiplying the probability to hop upward in energy with the Boltzmann factor, leading to significant computational savings.[16,17]

C. Simulation Details

The electronic structure calculations, geometry optimization and ground state molecular dynamics were carried out using the QE package. The electronic exchange and correlation interactions were treated using the Perdew-Burke-Ernzerhof (PBE) DFT functional.[20] The interactions of valence electrons with ions were accounted for via the projector augmented wave (PAW) method.[21] The van der Waals (vdW) interactions were included using the DFT-D3 approach. Pure DFT functionals, such as PBE, often underestimate energy gaps due to the self-interaction error. To account for this problem, the DFT+U approach was used, with U = 9.0 eV applied to the $3d$ electrons of the Ti atoms, improving description of the TiO_x electronic structure.[22] A basis set energy cutoff of 40 Ry and a kinetic energy cutoff of 400 Ry for charge density were employed. The simulation cells are shown in Fig. S3. The calculations were performed using a uniform $5 \times 5 \times 1$ k-point grid. Atomic positions were fully relaxed until the calculated Hellmann-Feynman forces were smaller than 0.05 eV/Å. After the structure optimization, repeated velocity rescaling was used to heat the systems to 300 K. Subsequently, 3 ps adiabatic MD trajectories were generated with a 1 fs atomic time step and were used for the NAMD calculations. The first 500 structures were used as initial

conditions to perform FSSH, with 1000 random number sequences for each structure, using the PYXAID package.

REFERENCES

[1] E. L. Radue, J. A. Tomko, A. Giri, J. L. Braun, X. Zhou, O. V. Prezhdo, E. L. Runnerstrom, J. P. Maria, and P. E. Hopkins, "Hot Electron Thermoreflectance Coefficient of Gold during Electron-Phonon Nonequilibrium," *ACS Photonics*, vol. 5, no. 12, pp. 4880–4887, 2018.

[2] D. H. Olson, K. M. Freedy, S. J. McDonnell, and P. E. Hopkins, "The influence of titanium adhesion layer oxygen stoichiometry on thermal boundary conductance at gold contacts," *Applied Physics Letters*, vol. 112, no. 171602, 2018.

[3] P. B. Johnson and R. W. Christy, "Optical Constant of the Nobel Metals," *Physical Review B*, vol. 6, no. 12, pp. 4370–4379, 1972.

[4] Z. Lin, L. V. Zhigilei, and V. Celli, "Electron-phonon coupling and electron heat capacity of metals under conditions of strong electron-phonon nonequilibrium," *Physical Review B*, vol. 77, no. 075133, 2008.

[5] J. Hohlfeld, S.-S. Wellershoff, J. Gudde, U. Conrad, V. Jahnke, and E. Matthias, "Electron and lattice dynamics following optical excitation of metals," *Chemical Physics*, vol. 251, pp. 237–258, 2000.

[6] B. C. Gundrum, D. G. Cahill, and R. S. Averback, "Thermal conductance of metal-metal interfaces," *Physical Review B - Condensed Matter and Materials Physics*, vol. 72, no. 24, 2005.

[7] R. W. Powell and R. P. Tye, "The thermal and electrical conductivity of titanium and its alloys," *Journal of the Less Common Metals*, vol. 3, no. 3, pp. 226–233, 1961.

[8] E. A. Scott, J. T. Gaskins, S. W. King, and P. E. Hopkins, "Thermal conductivity and thermal boundary resistance of atomic layer deposited high-k dielectric aluminum oxide, hafnium oxide, and titanium oxide thin films on silicon," *APL Materials*, vol. 6, no. 5, 2018.

[9] C. Kittel, *Introduction to solid state*, vol. 162. John Wiley & Sons, 1966.

[10] S. D. Brorson, A. Kazeroonian, J. S. Moodera, D. W. Face, T. K. Cheng, E. P. Ippen, M. S. Dresselhaus, and G. Dresselhaus, "Femtosecond room-temperature measurement of the electron-phonon coupling constant γ in metallic superconductors," *Physical Review Letters*, vol. 64, pp. 2172–2175, apr 1990.

[11]G.-M. Choi, R. B. Wilson, and D. G. Cahill, "Indirect heating of Pt by short-pulse laser irradiation of Au in a nanoscale Pt/Au bilayer," *Physical Review B*, vol. 89, no. 6, p. 64307, 2014.

[12]H. Jang, J. Kimling, and D. G. Cahill, "Nonequilibrium heat transport in Pt and Ru probed by an ultrathin Co thermometer," *Physical Review B*, vol. 101, no. 6, 2020.

[13]G. Chen and C. L. Tien, "Internal reflection effects on transient photothermal reflectance," *Journal of Applied Physics*, vol. 73, no. 7, pp. 3461–3466, 1993.

[14]R. B. Wilson, B. A. Apgar, L. W. Martin, and D. G. Cahill, "Thermoreflectance of metal transducers for optical pump-probe studies of thermal properties," *Optics Express*, vol. 20, no. 27, pp. 2267–2269, 2012.

[15]R. J. Stoner and H. J. Maris, "Kapitza conductance and heat flow between solids at temperatures from 50 to 300 K," *Physical Review B*, vol. 48, no. 22, pp. 16373–16387, 1993.

[16]A. V. Akimov and O. V. Prezhdo, "The PYXAID program for non-adiabatic molecular dynamics in condensed matter systems," *Journal of Chemical Theory and Computation*, vol. 9, no. 11, pp. 4959–4972, 2013.

[17]A. V. Akimov and O. V. Prezhdo, "Advanced capabilities of the PYXAID program: Integration schemes, decoherence effects, multiexcitonic states, and field-matter interaction," *Journal of Chemical Theory and Computation*, vol. 10, no. 2, pp. 789–804, 2014.

[18]P. Giannozzi, S. Baroni, N. Bonini, M. Calandra, R. Car, C. Cavazzoni, D. Ceresoli, G. L. Chiarotti, M. Cococcioni, I. Dabo, A. Dal Corso, S. De Gironcoli, S. Fabris, G. Fratesi, R. Gebauer, U. Gerstmann, C. Gougoussis, A. Kokalj, M. Lazzeri, L. Martin-Samos, N. Marzari, F. Mauri, R. Mazzarello, S. Paolini, A. Pasquarello, L. Paulatto, C. Sbraccia, S. Scandolo, G. Sclauzero, A. P. Seitsonen, A. Smogunov, P. Umari, and R. M. Wentzcovitch, "QUANTUM ESPRESSO: A modular and open-source software project for quantum simulations of materials," *Journal of Physics Condensed Matter*, vol. 21, no. 39, 2009.

[19]J. C. Tully, "Molecular dynamics with electronic transitions," *The Journal of Chemical Physics*, vol. 93, no. 2, pp. 1061–1071, 1990.

[20]J. P. Perdew, K. Burke, and M. Ernzerhof, "Generalized gradient approximation made simple," *Physical Review Letters*, vol. 77, no. 18, pp. 3865–3868, 1996.

[21]G. Kresse and D. Joubert, "From ultrasoft pseudopotentials to the projector augmented-wave method," *Physical Review B - Condensed Matter and Materials Physics*, vol. 59, no. 3, pp. 1758–1775, 1999.

[22]N. Nehaoua, R. Belkada, R. Z. Tala-Ighil, L. Thomas, R. Chemam, and D. E. Mekki, "Adsorption and dissociation of H_2S on the anatase TiO_2 (100) surface: DFT + U study," *Materials Research Express*, vol. 6, no. 2, 2019.